The dynamic modeling, redundant-force optimization, and dynamic performance analyses of a parallel kinematic machine with actuation redundancy

Yao Jiang, Tiemin Li* and Liping Wang

Department of Mechanical Engineering, Manufacturing Engineering Institute, Tsinghua University, Beijing 100084, China

SUMMARY
This paper discusses a planar 2-DOF (degrees of freedom) parallel kinematic machine with actuation redundancy. Its inverse dynamic model is constructed by utilizing the Newton–Euler method based on the kinematic analysis. However, the dynamic model cannot be solved directly because the number of equations is less than the number of unknowns, which is due to the redundant force. In order to solve this problem, the relationship between the deformations of the links and the position errors of the moving platform are further explored. Then a novel method, which aims at minimizing the position errors of the machine, is proposed to optimize the redundant force. It also enables to solve the dynamic model. Finally, the dynamic performance analyses of this machine and its non-redundant counterpart are provided by numerical examples. Besides, another optimization method proposed for minimizing the constraint forces is also applied for comparison. The results show the effectiveness of the novel methods in improving the position precision of the machine.

KEYWORDS: Parallel kinematic machine; Actuation redundancy; Dynamic modeling; Redundant-force optimization; Dynamic performance analysis.

1. Introduction
Parallel kinematic machine, which can be called PKM in short, appears as a new type of machine in recent decades. It possesses many advantages compared with the serial machine, such as high stiffness, rapid response, and large payload capacity.[1−3] Due to these potential advantages, the PKM has already drawn great attention of numerous researchers and been applied to industrial fields extensively.[4] With further research, however, the PKM has been found suffering from some drawbacks, including relatively small useful workspace, complex singularities, deformation and vibration of kinematic chains, and so on. The appearance of actuation redundancy[5−7] in a PKM can be an effective way to conquer these problems. A reasonable control of the redundant force will reduce or eliminate singularities, enhance stiffness, and improve precision.[8−11] However, an improper control without optimization will generate additional internal forces, greater consumption of servo motors, and even damage to the machine. Therefore, it is of great importance to optimize the redundant force for increasing the performance of the actuation-redundant PKM.

The introduction of actuation redundancy makes a PKM become an over-constraint machine. So its dynamic modeling will be noticeably complicated. The popular dynamic modeling methods for general PKMs include the Newton–Euler method,[12−15] the Lagrange method,[16,17] the principle of virtual work,[18,19] the Kane Equation,[20,21] and the screw theory method.[22] Nevertheless, all these methods, when used in the dynamic modeling of an actuation-redundant PKM, will lead to the result that the number of equations is less than the number of unknowns. It results in the non-unique solution of the dynamic model, which turns out to be a challenging task.

* Corresponding author. E-mail: litm@tsinghua.edu.cn

To solve this problem, some appropriate supplementary conditions should be found. Currently, the primary solution is establishing performance criteria to optimize the redundant force. Once the redundant force is obtained, the dynamic model can also be solved. Zheng[23] provided two methods to solve the load distribution problem for two coordinating industrial robots handling a single object, which could be deemed to be an actuation-redundant machine. The first method selected least energy consumption as the optimization criterion, and the other method was proposed for minimizing exerted forces on the object. The result showed the second method was more effectiveness and suitable for real-time application. Tao[24] minimized the square of the joint torques to resolve a similar problem. Nahon[25] used the quadratic programming approach with constraints to solve the problem of a hand grasping an object as an actuation-redundant kinematic chain. This approach allowed them to obtain minimum internal forces. Merlet[26] presented two solutions to obtain optimized redundant force: one for minimizing the joint rates and the other for minimizing the actuator torques, which were all based on the pseudo-inverse solution. Nokleby and Garg[9,27] presented an optimization-based solution to determine the force capabilities of actuation-redundant PKM. Their result showed that this method could make better use of the maximum torque/force capabilities of the actuators when compared to the non-redundant PKM and the pseudo-inverse solution. Lee[28] used the redundant force to produce an effective spring effect by proper internal load distribution. A methodology for optimal kinematic design of antagonistic stiffness was proposed and a five-bar mechanism was developed for experimental verification.

All these methods mentioned above are feasible in solving the optimization of the redundant force. However, there is no literature considering minimizing the position errors of the moving platform, which is extremely crucial in advanced PKMs. Furthermore, the kinematic chains of PKMs are generally composed of elongated rods, so they are easy to deform under external loads, which will reduce the position precision of the machine.[29,30] Therefore, it is necessary and feasible to improve the precision by optimizing the redundant force for actuation-redundant PKM.

In this paper, the dynamic modeling and redundant-force optimization of a planar 2-DOF (degrees of freedom) PKM with actuation redundancy are studied. The dynamic model of this machine is constructed by the Newton–Euler method. Then a novel redundant-force optimization method is proposed to minimize the position errors of the moving platform. A matrix, which is called position precision matrix in this paper, is obtained in the process of the optimization. It can reflect the machine's capability of resisting deformations to a certain extent. For the sake of verifying the effectiveness of this method, the dynamic performance of this machine and its non-redundant counterpart when running the selected trajectory is investigated by numerical examples. The analyses include the performance of their position precision matrixes, position and tracking errors, driving parameters, and constraint forces of joints. Finally, another redundant-force optimization method for minimizing the constraint forces is also applied for comparison.

2. Inverse Kinematic Analysis

2.1. Description of the actuation-redundant PKM
Figure 1 shows the schematic diagram of a planar 2-DOF actuation-redundant PKM. The machine is composed of a moving platform, two vertical rails, four identical links, and three sliders. The moving platform $A_1 A_2 A_3 A_4$ takes the form of a square. The links $A_1 B_1$ and $A_2 B_2$ connect the moving platform at points A_1 and A_2 to the slider P_1 at points B_1 and B_2 by revolute joints, respectively. The other two links $A_3 B_3$ and $A_4 B_4$ connect the moving platform at points A_3 and A_4 to the sliders P_2 and P_3 at points B_3 and B_4 by revolute joints, respectively. The motion of each slider is controlled by a corresponding servo motor when it moves along the rail, thus to drive the links to control the motion of the moving platform. There exists a parallelogram mechanism which limits the rotation of the moving platform. So, this machine possesses two translational degrees of freedom. The link $A_4 B_4$ and the slider P_3 comprise an actuation-redundant kinematic chain. Near point A_4, a force sensor is installed on link $A_4 B_4$. It is designed for the force closed-loop control, so that the servo motor can apply a predetermined force to the moving platform at point A_4 along the direction of $A_4 B_4$.

2.2. Inverse kinematics
As illustrated in Fig. 2, a reference coordinate frame $\{O\}\{O-XYZ\}$ is located at the midpoint of $C_1 C_2$, a moving coordinate frame $\{T\}\{T-xyz\}$ is attached to the moving platform at its
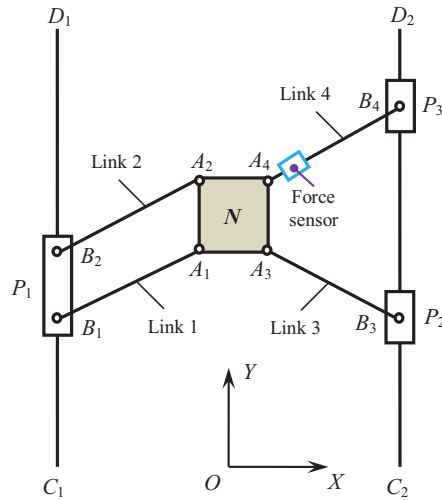
Fig. 1. Schematic diagram of the machine.
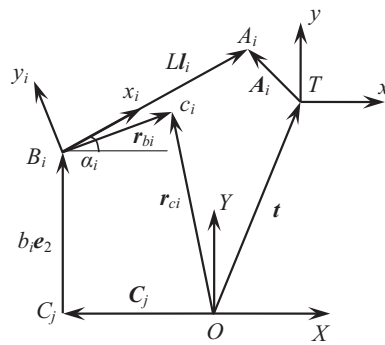
Fig. 2. Vector loop of a specific kinematic chain.

central point, and another moving coordinate frame $\{B_i\}\{B_i - x_i y_i z_i\}$ is attached to link $A_i B_i$ at point B_i.

The rotation matrixes of the coordinate frames $\{T\}$ and $\{B_i\}$ with respect to $\{O\}$ can be described respectively as

$$^O R_T = I_{3\times3} \tag{1}$$

and

$$^O R_{Bi} = [R_{ix}, R_{iy}, R_{iz}] = \begin{bmatrix} \cos\alpha_i & -\sin\alpha_i & 0 \\ \sin\alpha_i & \cos\alpha_i & 0 \\ 0 & 0 & 1 \end{bmatrix}, \tag{2}$$

where α_i is the angle between the x_i-axis and the X-axis.

According to Fig. 2, the vector loop equation for the ith kinematic chain can be written as

$$t + {}^O R_T {}^T A_i = C_j + b_i e_2 + Ll_i, \tag{3}$$

where $t = [x, y, 0]^T$, $^T A_i = [^T x_{Ai}, {}^T y_{Ai}, 0]^T$, and $C_j = [x_{Cj}, y_{Cj}, 0]^T$ $(j = 1, 2)$ are the position vectors of points T, A_i, and C_j in coordinate frames $\{O\}$, $\{T\}$, and $\{O\}$, respectively. Besides, $e_2 = [0, 1, 0]^T$ is the unit vector of vertical rail, and b_i is the distance between points B_i and C_j. L is the length of link $A_i B_i$, and l_i is the unit vector of the link in coordinate frame $\{O\}$, which can be expressed as

$$l_i = [l_{ix}, l_{iy}, 0]^T = R_{ix} = [\cos\alpha_i \quad \sin\alpha_i \quad 0]^T. \tag{4}$$

When the position vector t is given, the inverse kinematics can be determined uniquely based on the assembled mode in Fig. 1. Then l_i and b_i can be calculated according to Eq. (3).

The position vector of centroid c_i of link $A_i B_i$ in coordinate frames $\{B_i\}$ and $\{O\}$ can be expressed respectively as

$$^{Bi}\boldsymbol{r}_{ci} = \frac{L}{2}[1, 0, 0]^{\mathrm{T}} \tag{5}$$

and

$$\boldsymbol{r}_{ci} = \boldsymbol{C}_j + b_i\,\boldsymbol{e}_2 + {}^O\boldsymbol{R}_{Bi}{}^{Bi}\boldsymbol{r}_{ci}. \tag{6}$$

Differentiating Eq. (3) with respect to time yields

$$\boldsymbol{v}_T = v_i\,\boldsymbol{e}_2 + L\,(\boldsymbol{\omega}_i \times \boldsymbol{l}_i)\,, \tag{7}$$

where $\boldsymbol{v}_T = \dot{\boldsymbol{t}} = [v_{Tx}, v_{Ty}, 0]^{\mathrm{T}}$ is the velocity of point T, v_i is the velocity magnitude of point B_i, and $\boldsymbol{\omega}_i$ is the angular velocity of link $A_i B_i$.

Taking dot product and cross multiplication of Eq. (7) with l_i at both sides, we can obtain the velocity magnitude of point B_i and the angular velocity of link $A_i B_i$ respectively as

$$v_i = \frac{\boldsymbol{l}_i \cdot \boldsymbol{v}_T}{\boldsymbol{l}_i \cdot \boldsymbol{e}_2} \tag{8}$$

and

$$\boldsymbol{\omega}_i = \frac{1}{L}\,[\boldsymbol{l}_i \times (\boldsymbol{v}_T - v_i\boldsymbol{e}_2)]\,. \tag{9}$$

Taking the derivative of Eq. (6) with respect to time, we can obtain the velocity of point c_i as

$$\boldsymbol{v}_{ci} = v_i\,\boldsymbol{e}_2 + \boldsymbol{\omega}_i \times \left({}^O\boldsymbol{R}_{Bi}{}^{Bi}\boldsymbol{r}_{ci}\right). \tag{10}$$

Differentiating Eq. (7) with respect to the time yields

$$\boldsymbol{a}_T = a_i\,\boldsymbol{e}_2 + L\,(\boldsymbol{\varepsilon}_i \times \boldsymbol{l}_i) + \boldsymbol{\omega}_i \times (\boldsymbol{\omega}_i \times (L\boldsymbol{l}_i))\,, \tag{11}$$

where $\boldsymbol{a}_T = \dot{\boldsymbol{v}}_T = [a_{Tx}, a_{Ty}, 0]^{\mathrm{T}}$ is the acceleration of point T, a_i is the acceleration magnitude of point B_i, and $\boldsymbol{\varepsilon}_i$ is the angular acceleration of link $A_i B_i$.

Using the same method as above, the acceleration magnitude of point B_i, the angular acceleration of link $A_i B_i$, and the acceleration of point c_i can be calculated respectively as

$$a_i = \frac{\boldsymbol{l}_i \cdot \boldsymbol{a}_T + \left(\boldsymbol{\omega}_i^{\mathrm{T}}\boldsymbol{\omega}_i\right)L}{\boldsymbol{l}_i \cdot \boldsymbol{e}_2}, \tag{12}$$

$$\boldsymbol{\varepsilon}_i = \frac{1}{L}\boldsymbol{l}_i \times (\boldsymbol{a}_T - a_i\boldsymbol{e}_2)\,, \text{ and} \tag{13}$$

$$\boldsymbol{a}_{ci} = a_i\,\boldsymbol{e}_2 + \boldsymbol{\varepsilon}_i \times \left({}^O\boldsymbol{R}_{Bi}{}^{Bi}\boldsymbol{r}_{ci}\right) + \boldsymbol{\omega}_i \times \left(\boldsymbol{\omega}_i \times \left({}^O\boldsymbol{R}_{Bi}{}^{Bi}\boldsymbol{r}_{ci}\right)\right). \tag{14}$$

3. Inverse Dynamic Modeling
The Newton–Euler method is widely used in the dynamic analysis of PKMs, in which the equations of the motion for each kinematic chain and the moving platform can be derived[31] and all the reaction forces of links can be computed, which are indispensable in solving their deformations. Therefore, the dynamic model of this machine is constructed by utilizing the Newton–Euler method and D'Alemblert principle. Inertial forces and moments are applied on link $A_i B_i$ and the moving platform. Their force analyses are shown in Figs. 3 and 4, respectively.
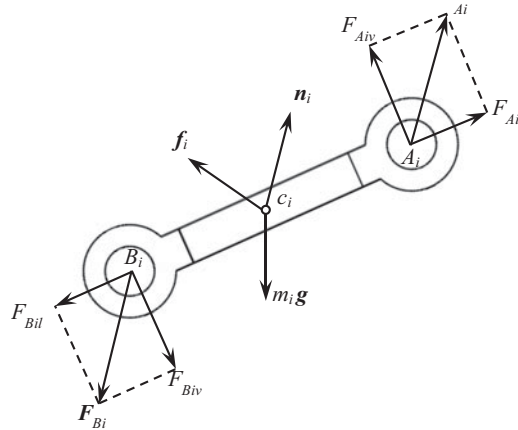
Fig. 3. Force analysis of link $A_i B_i$.
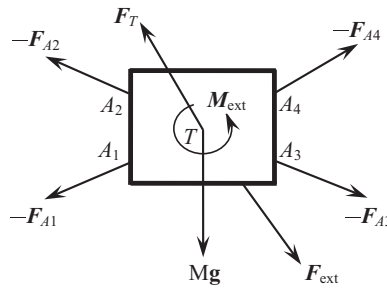
Fig. 4. Force analysis of the moving platform.

Referring to Fig. 3, the force balance equation of link $A_i B_i$ can be described as

$$\boldsymbol{F}_{Ai} + \boldsymbol{F}_{Bi} + m_i \boldsymbol{g} + \boldsymbol{f}_i = 0, \tag{15}$$

where m_i is the mass of link $A_i B_i$, $\boldsymbol{f}_i = -m_i \boldsymbol{a}_{ci}$ is its inertial force, and $\boldsymbol{F}_{Ai} = [F_{Aiv}, F_{Ail}, 0]^T$ and $\boldsymbol{F}_{Bi} = [F_{Biv}, F_{Bil}, 0]^T$ represent the constraint forces at points A_i and B_i, respectively.

Taking moment about point B_i, the moment balance equation of link $A_i B_i$ can be obtained as

$$\left({}^O\boldsymbol{R}_{Bi}{}^{Bi}\boldsymbol{r}_{ci}\right) \times (m_i \boldsymbol{g} + \boldsymbol{f}_i) + L\boldsymbol{l}_i \times \boldsymbol{F}_{Ai} + \boldsymbol{n}_i = 0, \tag{16}$$

where $\boldsymbol{n}_i = -\boldsymbol{J}_i \boldsymbol{\varepsilon}_i$ is the inertial moment of link $A_i B_i$, and $\boldsymbol{J}_i$ is its moment of inertia.

From Eq. (16) we can obtain F_{Aiv} as

$$F_{Aiv} = -\boldsymbol{e}_3^T[\boldsymbol{n}_i + \left({}^O\boldsymbol{R}_{Bi}{}^{Bi}\boldsymbol{r}_{ci}\right) \times (m_i \boldsymbol{g} + \boldsymbol{f}_i)]/L. \tag{17}$$

According to Fig. 4, the force balance equation of the moving platform can be described as

$$\mathrm{M}\boldsymbol{g} + \boldsymbol{F}_{\mathrm{ext}} + \boldsymbol{F}_T - \sum_{i=1}^{4} \boldsymbol{F}_{Ai} = 0, \tag{18}$$

where M is the mass of the moving platform, $\boldsymbol{F}_T = -\mathrm{M}\boldsymbol{a}_T$ is its inertial force, and $\boldsymbol{F}_{\mathrm{ext}} = [F_{\mathrm{ext}x}, F_{\mathrm{ext}y}, 0]^T$ is the external force acting on the moving platform.

Taking moment about point T, the moment balance equation of the moving platform can be obtained as

$$\left(^{O}\boldsymbol{R}_{T}\boldsymbol{R}\right) \times (\mathrm{M}\boldsymbol{g} + \boldsymbol{F}_{T}) - \sum_{i=1}^{4}\left(^{O}\boldsymbol{R}_{T}{}^{T}\boldsymbol{A}_{i}\right) \times \boldsymbol{F}_{Ai} + \boldsymbol{M}_{\mathrm{ext}} = 0, \tag{19}$$

where $\boldsymbol{R} = [^{T}R_{x}, {}^{T}R_{y}, 0]^{\mathrm{T}}$ is the position vector of the centroid of the moving platform in coordinate frame $\{T\}$, and $\boldsymbol{M}_{\mathrm{ext}}$ is the external moment acting on the moving platform.

Equations (18) and (19) can be simplified as

$$\boldsymbol{P}\begin{bmatrix} F_{A1l} & F_{A2l} & F_{A3l} \end{bmatrix}^{\mathrm{T}} = \boldsymbol{Q}, \tag{20}$$

where

$$\boldsymbol{P} = \begin{bmatrix} l_{1x} & l_{2x} & l_{3x} \\ l_{1y} & l_{2y} & l_{3y} \\ u_{1} & u_{2} & u_{3} \end{bmatrix},$$

$$\boldsymbol{Q} = \begin{bmatrix} F_{\mathrm{ext}x} - \mathrm{M}a_{Tx} + \sum_{i=1}^{4} l_{iy}F_{Aiv} - l_{4x}F_{A4l} \\ F_{\mathrm{ext}y} - \mathrm{M}g - \mathrm{M}a_{Ty} - \sum_{i=1}^{4} l_{ix}F_{Aiv} - l_{4y}F_{A4l} \\ {}^{T}R_{y}\mathrm{M}a_{Tx} - {}^{T}R_{x}(\mathrm{M}g + \mathrm{M}a_{Ty}) + M_{\mathrm{ext}} - \sum_{i=1}^{4} w_{i}\,F_{Aiv} - u_{4}F_{A4l} \end{bmatrix},$$

$$u_{i} = l_{iy}{}^{T}x_{Ai} - l_{ix}{}^{T}y_{Ai},\, w_{i} = l_{ix}{}^{T}x_{Ai} + l_{iy}{}^{T}y_{Ai}.$$

There are four unknowns (F_{Ail}) in Eq. (20), while the number of equations is three, so it is obvious that the dynamic model cannot be solved directly. Supplementary conditions should be added for solving this problem. Since the redundant force F_{A4l} can be controlled actively by the actuation-redundant kinematic chain, it can be optimized for the purpose of minimizing the running position errors of the moving platform, which will offer a feasible supplementary condition. In order to achieve this goal, the relationship between the position errors of the moving platform and the redundant force should be established.

4. Optimization of the Redundant Force

As for the machine, there are a large number of inevitable errors in the process of manufacturing and assembling, including the distance and parallelism between the two rails, the length of link $A_{i}B_{i}$, the installed position of point A_{i}, and so on. All these are static position errors, which can be calculated and compensated through kinematic calibration; while those errors of the moving platform, which are caused by the deformations of components during operation, are changing dynamically. So it is impossible to eliminate them by the conventional static compensation in advance. Due to the characteristic of those errors, they should be compensated in real time. The actuation redundancy will be an effective approach to minimize the dynamic errors through the optimization of the redundant force.

Considering the structural feature of this machine, the deformations of the rails, the sliders and the moving platform can be neglected. The deformations of the links are mainly to be taken into account here.

4.1. Relationship between the deformations of the links and the kinematic errors of the moving platform

Tension and compression deformation will occur in the links, which can be called as axial deformation and bending deformation during operation. As shown in Fig. 5, the axial deformation will lead to the axial error δL_{i} of link $A_{i}B_{i}$, and the bending deformation will lead to the angular error $\delta\alpha_{i}$ of link $A_{i}B_{i}$.

(a) Axial deformation diagram of link A_iB_i

(b) Bending deformation diagram of link A_iB_i
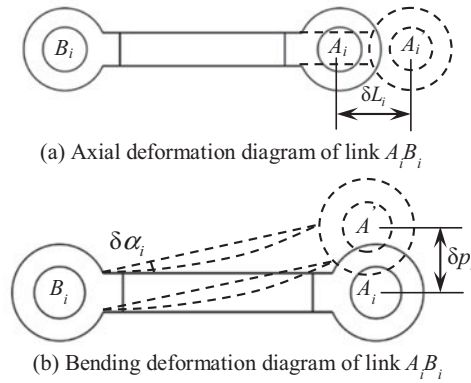
Fig. 5. Deformation diagrams of link A_iB_i.

Except for the redundant link A_4B_4 which is controlled by torque model, the deformations of links A_iB_i ($i = 1, 2, 3$) will lead to the kinematic errors of the moving platform. These errors include the position errors (δx and δy) and the rotation error ($\delta \theta$) which is perpendicular to the XY plane. Considering these errors, Eq. (3) should be rewritten as

$$\boldsymbol{t} + \delta \boldsymbol{t} + \left({}^O\boldsymbol{R}_T + \delta {}^O\boldsymbol{R}_T\right)^T \boldsymbol{A}_i = \boldsymbol{C}_j + b_i \boldsymbol{e}_2 + (L + \delta L_i)(\boldsymbol{l}_i + \delta \boldsymbol{l}_i), \tag{21}$$

where $\delta \boldsymbol{t} = [\delta x, \delta y, 0]^T$, $\delta {}^O\boldsymbol{R}_T = (\boldsymbol{WI})\,\delta\theta$, $\boldsymbol{W} = \begin{bmatrix} 0 & -1 & 0 \\ 1 & 0 & 0 \\ 0 & 0 & 0 \end{bmatrix}$, and $\delta \boldsymbol{l}_i = \delta \alpha_i [-\sin \alpha_i \ \cos \alpha_i \ 0]^T$.

Subtracting Eq. (3) from Eq. (21) and ignoring the higher order items yields

$$\delta \boldsymbol{t} + \delta {}^O\boldsymbol{R}_T^T \boldsymbol{A}_i = L\delta \boldsymbol{l}_i + \boldsymbol{l}_i \delta L_i. \tag{22}$$

Equation (22) reflects the relationship between the kinematic errors of the moving platform and deformations of the links. Considering that both ends of link A_iB_i are connected by revolute joints, the bending deformation can only occur under the gravity and inertia moment of the link, which are relatively smaller than constraint forces of the joints. Besides, the maximum bending deformation occurs near the middle of the link, so its influence on the error of the end point of the link is little. Therefore, in order to simplify the problem, only the axial deformations of the links will be investigated.

Taking dot product of Eq. (22) with $\boldsymbol{l}_i$ at both sides yields

$$\boldsymbol{l}_i \cdot \left(\delta \boldsymbol{t} + \delta {}^O\boldsymbol{R}_T^T \boldsymbol{A}_i\right) = \delta L_i. \tag{23}$$

The relationship between the axial deformations of the links and the kinematic errors of the moving platform can be obtained from Eq. (23) as

$$\boldsymbol{E}[\,\delta x \quad \delta y \quad \delta \theta\,]^T = [\,\delta L_1 \quad \delta L_2 \quad \delta L_3\,]^T, \tag{24}$$

where

$$\boldsymbol{E} = \begin{bmatrix} l_{1x} & l_{1y} & u_1 \\ l_{2x} & l_{2y} & u_2 \\ l_{3x} & l_{3y} & u_3 \end{bmatrix} = \boldsymbol{P}^T.$$

4.2. The axial deformation of the links
The force analysis diagram for solving the axial deformation of link A_iB_i is shown in Fig. 6, where $\boldsymbol{p}_i(x)$ represents the distributed load on the link, including the gravity and inertial force, which can
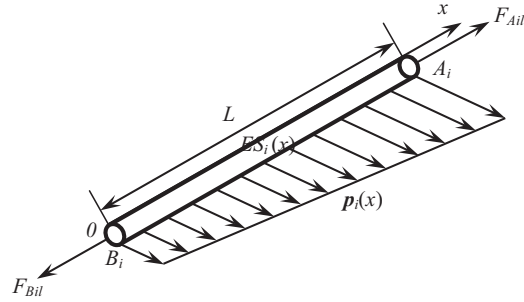
Fig. 6. Force analysis diagram of link $A_i B_i$.

be described as

$$p_i(x) = \frac{m_i(g - a_{xi})}{L} = \frac{m_i\left(g - \left(a_{Bi} + \varepsilon_i \times (xl_i) - \left(\omega_i^{\mathrm{T}}\omega_i\right) \cdot (xl_i)\right)\right)}{L}. \tag{25}$$

Setting point B_i as the origin, the axial force F_{dx} of link $A_i B_i$ at coordinate x can be written as

$$F_{dx} = \int_x^L \left(l_i^{\mathrm{T}} p_i(x)\right) dx + F_{Ail}. \tag{26}$$

The axial deformation of link $A_i B_i$ can be described as

$$\delta L_i = \int_0^L \frac{F_{dx} dx}{E S_i(x)} = \int_0^L \frac{\int_x^L \left(l_i^{\mathrm{T}} p_i(x)\right) dx + F_{Ail}}{E S_i(x)} dx, \tag{27}$$

where $S_i(x)$ is the cross-sectional area of the link at coordinate x and E is the elastic modulus.

The cross-sectional area $S_i(x)$ is considered to be constant along the longitudinal direction of the link. From Eq. (27) we can yield

$$\delta L_i = \int_0^L \frac{\int_x^L \left(l_i^{\mathrm{T}}\left(m_i\left(g - \left(a_{Bi} + \varepsilon_i \times (xl_i) - \left(\omega_i^{\mathrm{T}}\omega_i\right) \cdot (xl_i)\right)\right)\right)\right) dx + F_{Ail}L}{E S_i L} dx$$

$$= \frac{L}{6E S_i}\left(3m_i l_i^{\mathrm{T}}(g - a_{Bi}) + m_i\left(\omega_i^{\mathrm{T}}\omega_i\right) L + 6F_{Ail}\right). \tag{28}$$

Substituting Eq. (28) in Eq. (24) yields

$$E \begin{bmatrix} \delta x \\ \delta y \\ \delta \theta \end{bmatrix} = \begin{bmatrix} \dfrac{L}{6E S_1}\left(3m_1 l_1^{\mathrm{T}}(g - a_{B1}) + m_1\left(\omega_1^{\mathrm{T}}\omega_1\right) L + 6F_{A1l}\right) \\[2ex] \dfrac{L}{6E S_2}\left(3m_2 l_2^{\mathrm{T}}(g - a_{B2}) + m_2\left(\omega_2^{\mathrm{T}}\omega_2\right) L + 6F_{A2l}\right) \\[2ex] \dfrac{L}{6E S_3}\left(3m_3 l_3^{\mathrm{T}}(g - a_{B3}) + m_3\left(\omega_3^{\mathrm{T}}\omega_3\right) L + 6F_{A3l}\right) \end{bmatrix}. \tag{29}$$

4.3. Optimization of the redundant force

The above analyses show that the deformation of the links leads to the position errors and the rotation error of the moving platform during operation. Among them, the rotation error does not affect the precision of the center of the moving platform, so that the optimization goal can be defined as

$$H = \min \sqrt{(\delta x)^2 + (\delta y)^2}. \tag{30}$$

In order to obtain a satisfied redundant force F_{A4l}, Eq. (30) should be represented in the expression of F_{A4l}.

Equation (29) can be written as a general form of

$$F = KED + G, \tag{31}$$

where

$$F = \begin{bmatrix} F_{A1l} & F_{A2l} & F_{A3l} \end{bmatrix}^{\mathrm{T}},$$

$$D = \begin{bmatrix} \delta x & \delta y & \delta\theta \end{bmatrix}^{\mathrm{T}},$$

$$K = \begin{bmatrix} \dfrac{E S_1}{L} & 0 & 0 \\ 0 & \dfrac{E S_2}{L} & 0 \\ 0 & 0 & \dfrac{E S_3}{L} \end{bmatrix},$$

$$G = \begin{bmatrix} -\dfrac{m_1}{6} \left(3l_1^{\mathrm{T}} (g - a_{B1}) + (\omega_1^{\mathrm{T}}\omega_1) L \right) \\ -\dfrac{m_2}{6} \left(3l_2^{\mathrm{T}} (g - a_{B2}) + (\omega_2^{\mathrm{T}}\omega_2) L \right) \\ -\dfrac{m_3}{6} \left(3l_3^{\mathrm{T}} (g - a_{B3}) + (\omega_3^{\mathrm{T}}\omega_3) L \right) \end{bmatrix}.$$

Substituting Eq. (31) in Eq. (20) yields

$$E^{\mathrm{T}} (KED + G) = Q. \tag{32}$$

The kinematic errors of the moving platform can be obtained from Eq. (32) as

$$D = E^{-1}K^{-1} \left(E^{-\mathrm{T}}Q - G \right) = RQ + N, \tag{33}$$

where $R = E^{-1}K^{-1}E^{-\mathrm{T}}$ and $N = -E^{-1}K^{-1}G$.

Substituting Eq. (33) in Eq. (30), we can obtain the optimization objective function H as

$$H = f(F_{A4l}) = \sqrt{a F_{A4l}^2 + b F_{A4l} + c}, \tag{34}$$

where

$$a = a_1^2 + a_2^2 \geq 0,$$
$$b = 2 (a_1 b_1 + a_2 b_2),$$
$$c = b_1^2 + b_2^2,$$
$$a_1 = -r_{11} l_{4x} - r_{12} l_{4y} - r_{13} u_4,$$
$$a_2 = -r_{21} l_{4x} - r_{22} l_{4y} - r_{23} u_4,$$
$$b_1 = r_{11} q_1 + r_{12} q_2 + r_{13} q_3 + n_1,$$
$$b_2 = r_{21} q_1 + r_{22} q_2 + r_{23} q_3 + n_2,$$

$$q_1 = F_{\text{ext}x} - Ma_{Tx} + \sum_{i=1}^{4} l_{iy} F_{Aiv},$$

$$q_2 = F_{\text{ext}y} - Mg - Ma_{Ty} - \sum_{i=1}^{4} l_{ix} F_{Aiv},$$

$$q_3 = {}^T R_y Ma_{Ty} - {}^T R_x (Mg + Ma_{Ty}) + M_{\text{ext}} - \sum_{i=1}^{4} w_i F_{Aiv}.$$

$r_{11}, r_{12}, r_{13}, r_{21}, r_{22}, r_{23}$ are the components of matrix R and n_1, n_2, n_3 are the components of matrix N.

Referring to Eq. (34), the optimal value of force F_{A4l} will be discussed as follows:

$$F_{A4l} = \begin{cases} -\dfrac{b}{2a}, & a > 0 \\ F_{\min}, & a = 0 \quad \text{and} \quad b > 0 \\ F_{\max}, & a = 0 \quad \text{and} \quad b < 0 \\ 0, & a = 0 \quad \text{and} \quad b = 0 \end{cases} \tag{35}$$

where $F_{\max}$ and $F_{\min}$ represent the maximum and minimum axial forces provided by the actuation-redundant kinematic chain, respectively.

Substituting F_{A4l} in Eq. (33), we can obtain the kinematic errors of the moving platform, and then forces F_{Ail} ($i = 1, 2, 3$) can be calculated by using Eq. (31).

Then $\boldsymbol{F}_{Bi}$ can be obtained according to Eqs. (15) and (17) as

$$\boldsymbol{F}_{Bi} = -\boldsymbol{F}_{Ai} - m_i \boldsymbol{g} + m_i \boldsymbol{a}_{ci}. \tag{36}$$

Assuming that there is no friction between the sliders and the vertical rails, the force balance equations of the sliders can be described as

$$\boldsymbol{F}_{P1} - (\boldsymbol{F}_{B1} + \boldsymbol{F}_{B2}) + m_{s1}(\boldsymbol{g} - a_1 \boldsymbol{e}_2) = 0, \tag{37}$$

$$\boldsymbol{F}_{P2} - \boldsymbol{F}_{B3} + m_{s2}(\boldsymbol{g} - a_3 \boldsymbol{e}_2) = 0, \tag{38}$$

$$\boldsymbol{F}_{P3} - \boldsymbol{F}_{B4} + m_{s3}(\boldsymbol{g} - a_4 \boldsymbol{e}_2) = 0, \tag{39}$$

where $\boldsymbol{F}_{P1}$, $\boldsymbol{F}_{P2}$, and $\boldsymbol{F}_{P3}$ are the forces acting on the sliders P_1, P_2, and P_3, and m_{s1}, m_{s2}, and m_{s3} are the masses of the sliders P_1, P_2, and P_3.

The driving forces of the servo motors can be obtained from the components in the *Y*-direction of $\boldsymbol{F}_{P1}$, $\boldsymbol{F}_{P2}$, and $\boldsymbol{F}_{P3}$ as

$$F_{d1} = (F_{B1y} + F_{B2y}) + m_{s1}(g + a_1), \tag{40}$$

$$F_{d2} = F_{B3y} + m_{s2}(g + a_3), \tag{41}$$

$$F_{d3} = F_{B4y} + m_{s3}(g + a_4). \tag{42}$$

5. Simulation Analyses

The dynamic performance of the machine proposed and its non-redundant counterpart is analyzed by numerical examples in this section. Besides, another performance criterion for minimizing the constraint forces is also applied to optimize the redundant force for comparison.

Table I. The related parameters of the actuation-redundant PKM.

Parameters	Meanings	Values	Unit
M	Mass of the moving platform	3034	kg
m	Mass of the link	1985	kg
S_i	Cross-area of the link	0.075	m^2
J_i	Moment of inertia of the link	1856	kg·m^2
m_{s1}	Mass of slider P_1	1750	kg
m_{s2}	Mass of slider P_2	850	kg
m_{s3}	Mass of slider P_3	850	kg
L_0	Length of the link	3.35	m
L_1	Distance between the vertical rails	4.2	m
L_2	Side length of the moving platform	0.8	m
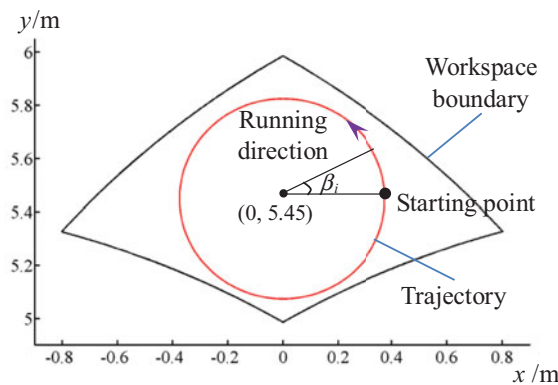
Fig. 7. Workspace and trajectory.

The related parameters of the actuation-redundant PKM are shown in Table I. Except for the redundant kinematic chain, the two machines are identical.

5.1. Trajectory planning

The trajectory of each moving platform should be provided to analyze the dynamic performance of these two machines. Since the redundant kinematic chain has no influence on the mobility of the machine, when the distance of the sliders P_1 and P_2 moving along the rails is 1 m, the workspace of the two machines is the same, as shown in Fig. 7. In the workspace, a circle is selected as the trajectory of the moving platform. The center point of the trajectory is at (0, 5.45) m, and the diameter is 0.75 m. The starting point and running direction are also shown in Fig. 7.

When the trajectory is determined, the accelerating characteristics are then analyzed. To avoid impact during operation, S-shape curve is used to plan the trajectory[32] and the acceleration of the moving platform can be illustrated as

$$
a = \begin{cases}
\dfrac{2a_0}{T}t & \left(0 \le t \le \dfrac{T}{2}\right) \\[2mm]
-\dfrac{2a_0}{T}t + 2a_0 & \left(\dfrac{T}{2} < t \le T\right) \\[2mm]
0 & (T < t \le T_t - T) \\[2mm]
-\dfrac{2a_0}{T}(t - T_t + T) & \left(T_t - T < t \le T_t - \dfrac{T}{2}\right) \\[2mm]
\dfrac{2a_0}{T}(t - T_t) & \left(T_t - \dfrac{T}{2} < t \le T_t\right)
\end{cases}, \qquad (43)
$$

(a) Condition number of matrix **R** of the
non-redundant PKM

(b) Condition number of matrix **R** of the
actuation redundant PKM
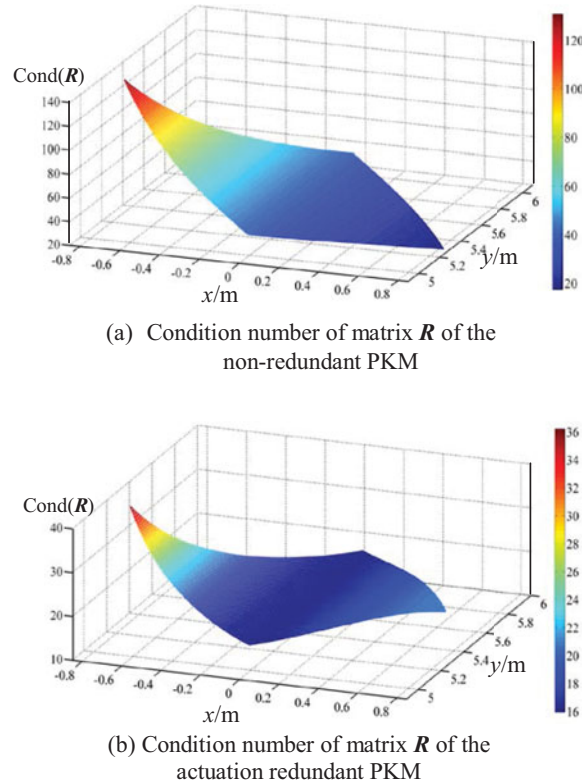
Fig. 8. Condition numbers of the position precision matrixes.

where a_0 is the maximum acceleration, T is the time in acceleration and deceleration stages, and T_t is the total running time. The velocity v and displacement s during operation can be obtained by integration. In this simulation, $a_0 = 0.25$ m/s^2 and $T = 2$ s.

5.2. Dynamic performance analyses of the two machines

In this section, the dynamic performance of the two machines will be analyzed for comparison to show the effect of the optimized redundant force on the actuation-redundant PKM. These analyses include the performance of their position precision matrixes, position and tracking errors, driving parameters, and constraint forces of joints.

Equation (33) shows that the position errors of the moving platform is determined by matrix R, named position precision matrix here. This matrix is only defined by the dimension parameters and the pose of the machine. Therefore, it is essential to select suitable dimension parameters and trajectories to guarantee the performance of matrix R, which will be beneficial to ensure high precision of the moving platform during operation. Otherwise, it will be difficult to compensate the position errors even if the actuation redundancy is introduced.

The performance of matrix R can be characterized by its condition number. The smaller the condition number is, the better performance the matrix has. The condition numbers of matrix R of the two machines in their workspaces are shown in Fig. 8. It can be seen that the condition number of matrix R of the actuation-redundant PKM is smaller, which indicates that the redundant kinematic chain improves the machine's capability of resisting deformations at a certain extent, thus ensuring a better position precision of the machine.

The condition numbers of matrix R of the two machines in the specified circular trajectory are shown in Fig. 9. It can be inferred that the position precision of the actuation-redundant PKM will be superior to the non-redundant one when running this trajectory.

To emphasize the role of the optimized redundant force in improving the position precision of the machine during operation, the position and tracking errors of these two machines when running the given circular trajectory will be computed.
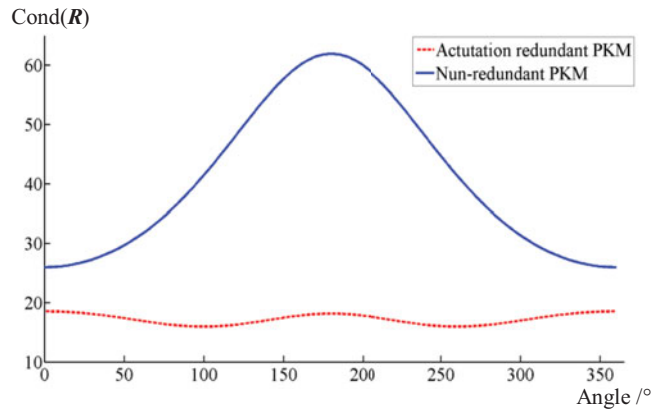
Fig. 9. Condition numbers of the position precision matrixes in circular trajectory.
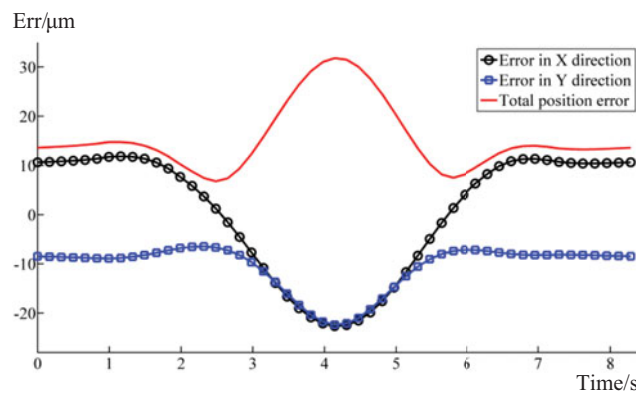
Fig. 10. Position errors of the non-redundant PKM.

The position errors in *X* and *Y* directions and the total position error of the non-redundant PKM when running the circular trajectory are shown in Fig. 10. It can be seen that the maximum position error of the center of the moving platform is nearly 32 μm and it occurs in the region where the condition number of matrix *R* is also at its maximum.

The tracking error is shown in Fig. 11. The red dotted line and the black solid line represent the ideal circular trajectory and the actual trajectory, respectively. To get a better view, the position error in actual trajectory is amplified to 1000 times.

The position and tracking errors of the actuation-redundant PKM with optimized redundant force when running the same circular trajectory are shown in Figs. 12 and 13, respectively. It can be seen that the position and tracking precision are all obviously improved and the maximum position error is reduced to less than 12 μm.

In order to obtain a better comparison of the dynamic performance of these two machines, their other important dynamic parameters, including driving parameters and constraint forces, are analyzed further.

The driving forces of the two machines when running the circular trajectory are shown in Figs. 14 and 15, respectively.

It shows that the maximum redundant driving force occurs in the region where the condition number of matrix *R* of the non-redundant PKM is also at its maximum. It can be concluded that the worse the performance of the machine is, the greater redundant driving force is needed to compensate for the position errors during operation.

The driving power of each motor of the two machines is given in Figs. 16 and 17, respectively.

In order to get a better comparison, the total driving power of the two machines is given in Fig. 18. It can be seen that the driving power of the actuation-redundant PKM is always bigger than the
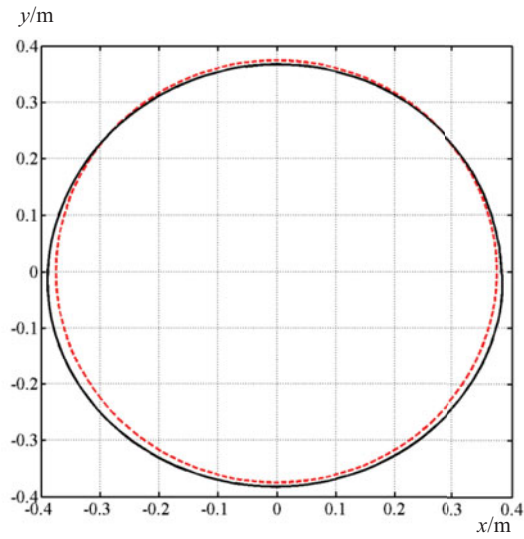
Fig. 11. Tracking error of the non-redundant PKM.
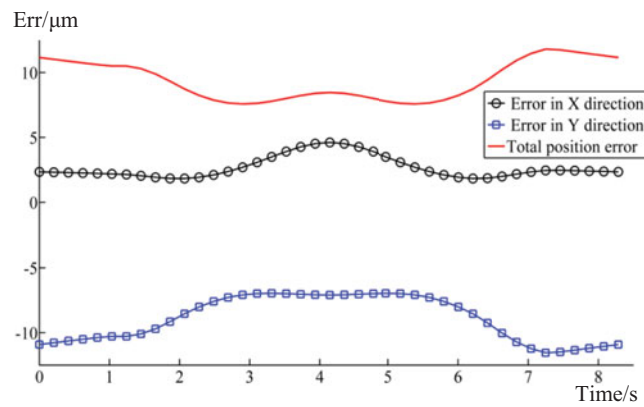
Fig. 12. Position errors of the actuation-redundant PKM.
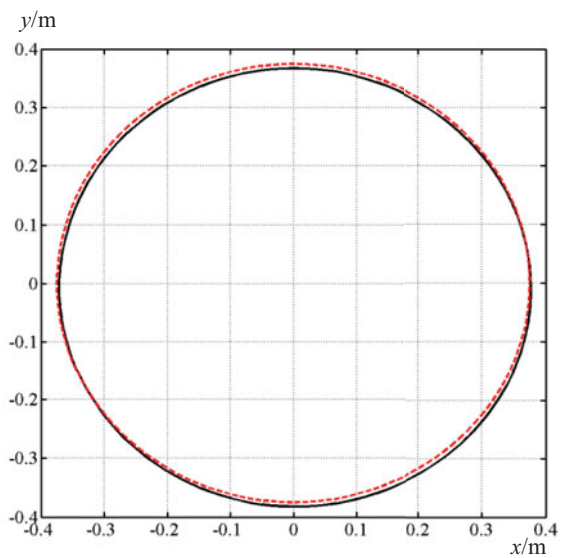
Fig. 13. Tracking error of the actuation-redundant PKM.
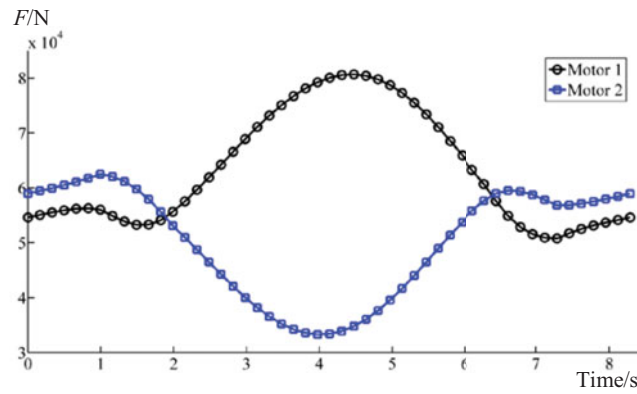
Fig. 14. Driving forces of the non-redundant PKM.
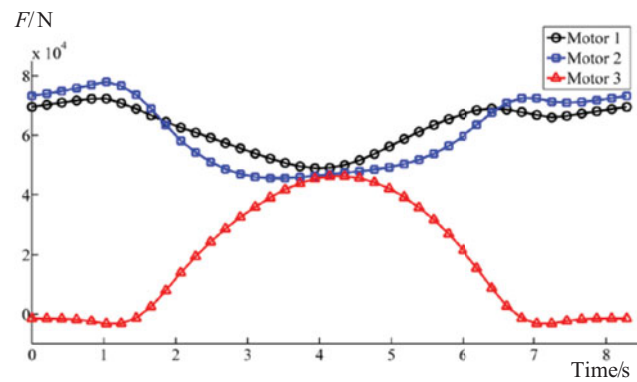
Fig. 15. Driving forces of the actuation-redundant PKM.
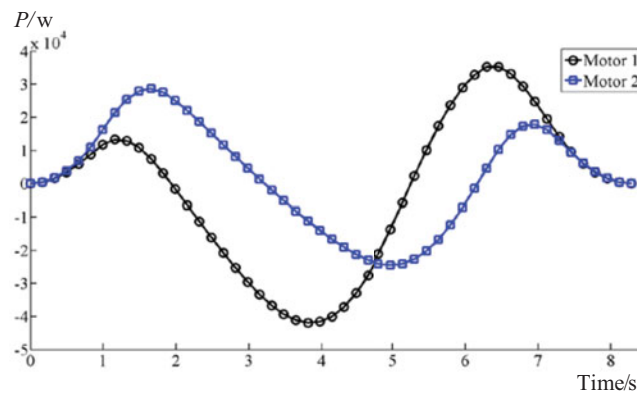
Fig. 16. Driving power of each motor of the non-redundant PKM.

non-redundant PKM. So the improved position precision of the actuation-redundant PKM is at the cost of more consumption.

Besides, the constraint forces of the joints of each link are analyzed. The constraint forces of joints A_i ($i = 1, 2, 3$) and joints B_i ($i = 1, 2, 3$) of the non-redundant PKM are given in Figs. 19 and 20, respectively.

The constraint forces of joints A_i ($i = 1, 2, 3, 4$) and joints B_i ($i = 1, 2, 3, 4$) of the actuation-redundant PKM are given in Figs. 21 and 22, respectively.

Through comparison we can find that the constraint forces of the actuation-redundant PKM are relatively larger at the start and end of the trajectory. However, because of the effect of the redundant force, its constraint forces reduce obviously at the middle of the trajectory, compared with the
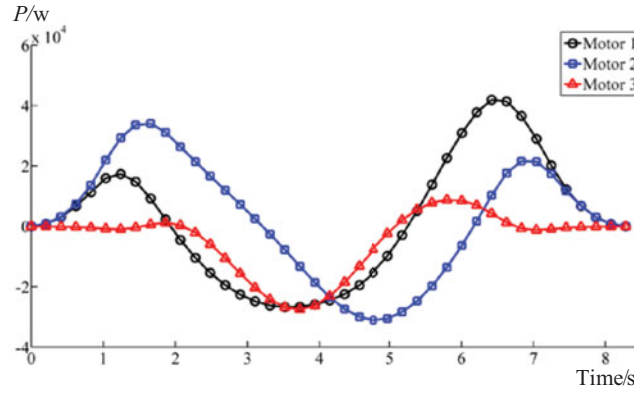
Fig. 17. Driving power of each motor of the actuation-redundant PKM.
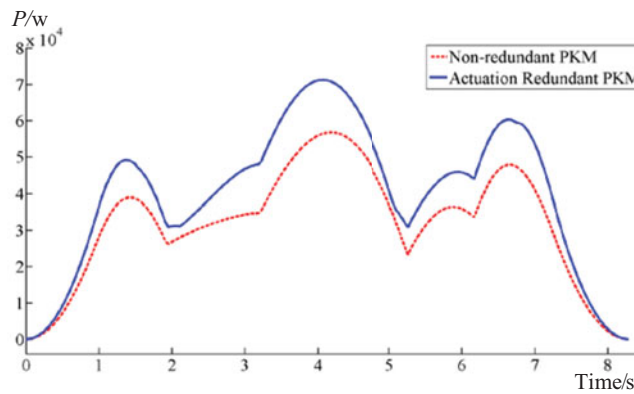
Fig. 18. Total driving power of each machine.
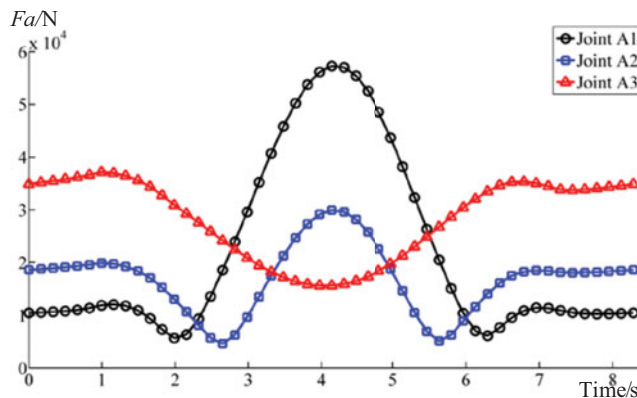
Fig. 19. Constraint forces of joints A_i of the non-redundant PKM.

non-redundant PKM, especially the constraint forces of joints A_1 and B_1. It shows the function of the redundant force in controlling the constraint forces to reduce the deformations of the links, thus contributing to improve the position precision of the machine.

5.3. Optimization method for minimizing the constraint forces
In order to illustrate the effectiveness of the method proposed in improving the position precision of the machine further, another redundant-force optimization method for minimizing the constraint forces is applied for comparison.[24,25] The constraint forces of joints A_i and B_i directly affect the deformations of the links, so they can also be minimized to improve the position precision of the
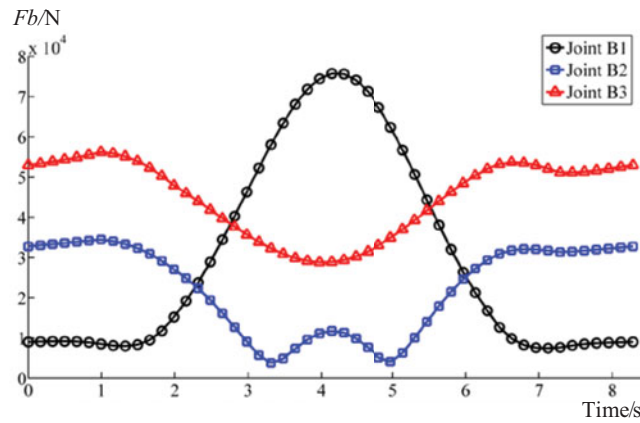
Fig. 20. Constraint forces of joints B_i of the non-redundant PKM.
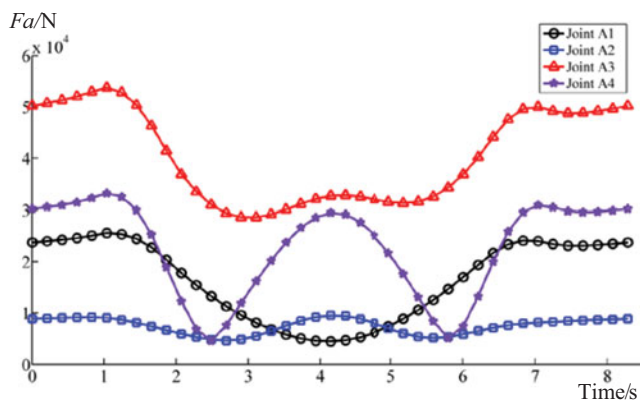
Fig. 21. Constraint forces of joints A_i of the actuation-redundant PKM.
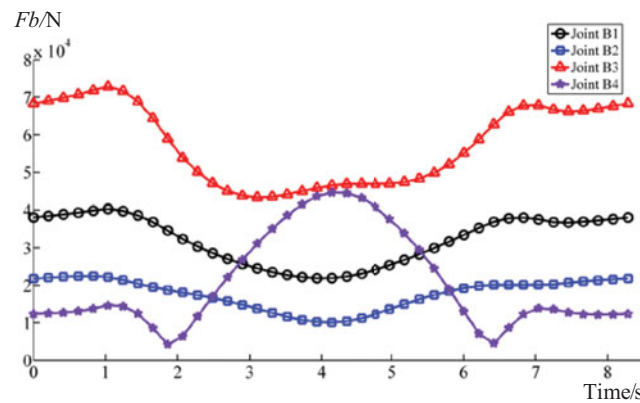
Fig. 22. Constraint forces of joints B_i of the actuation-redundant PKM.

machine. The optimization goal can be defined as

$$H' = \min \left(\sum_{i=1}^{4} (\|\boldsymbol{F}_{Ai}\| + \|\boldsymbol{F}_{Bi}\|) \right). \tag{44}$$

The method proposed before can be called as method I and this method can be called as method II. The constraint forces of joints A_i and joints B_i of the actuation-redundant PKM when using method II are given in Figs. 23 and 24, respectively. It can be seen that they are indeed smaller.
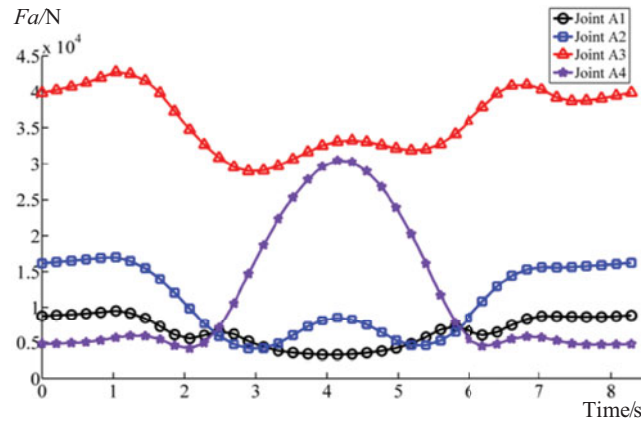
Fig. 23. Constraint forces of joints A_i of the actuation-redundant PKM when using method II.
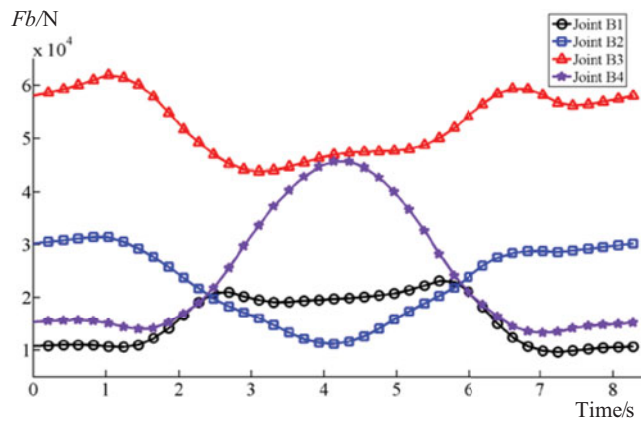
Fig. 24. Constraint forces of joints B_i of the actuation-redundant PKM when using method II.
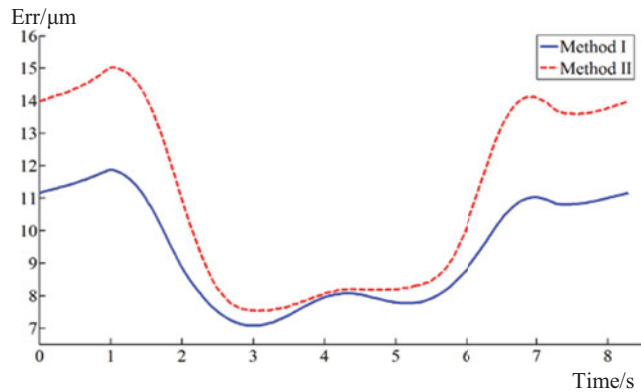
Fig. 25. Total position error of the actuation-redundant PKM when using the two methods.

The total position errors of the actuation-redundant PKM when using the two methods are all given in Fig. 25. The constraint forces when using method II are reduced, so the deformations of the links should be smaller and the position precision of the machine should be improved. However, it can be seen from Fig. 25 that the total position error of the actuation-redundant PKM when using method II is always bigger. It proves the effectiveness of method I in improving the position precision of the machine

The total driving power of the actuation-redundant PKM when using the two methods is given in Fig. 26. It shows that the consumption of the machine is nearly the same in both cases.
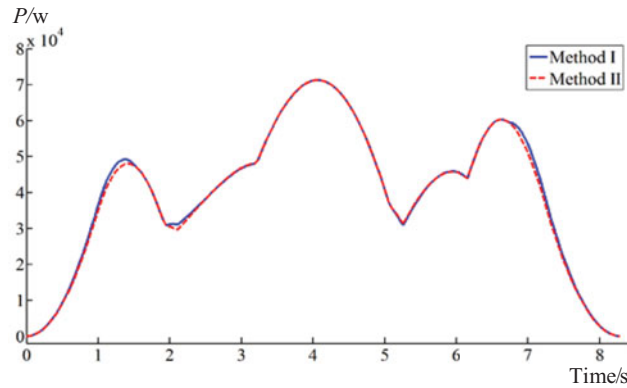
Fig. 26. Total driving power of the actuation-redundant PKM when using the two methods.
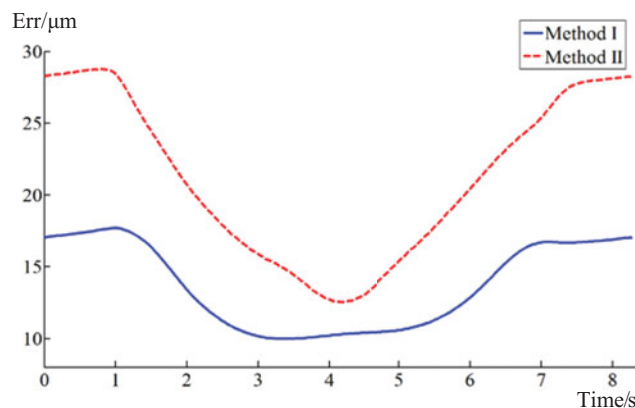
Fig. 27. Total position error of the actuation-redundant PKM under external loads.

When external load of $F = [4, 3] \times 10^4$ N is applied on the moving platform of the actuation-redundant PKM, the total position errors of the machine when using the two methods are provided in Fig. 27. It can be seen that the maximum position error of the machine using method II increases obviously, from 15 μm to nearly 30 μm. By contrast, the position error of the machine using method I is still relatively small and the maximum position error increases less than 6 μm. It well proves that method I can ensure that the machine possesses a better capacity in resisting external disturbance, thus obtaining higher position precision.

Another two trajectories are selected for analyzing the position errors of the two machines. The first one is still a circular trajectory with the same center point of the previous one, while its diameter is 1.5 m. The other one is a line trajectory, with its start point at (−1,−1) m and the end point at (1,1) m. The motion parameters and the external load when running these two trajectories remain unchanged.

The total position errors of the two machines when running the given trajectories are provided in Figs. 28 and 29, respectively. The results show the effectiveness of the novel method proposed in reducing the position error of the machine once more.

5.4. Insufficiency of the actuation redundancy
Expanding the diameter of the previous trajectory to 2.5 m, the position errors of the two machines are analyzed once more. The condition numbers of matrix *R* of the two machines in the expanded circular trajectory are shown in Fig. 30. It can be inferred that the performance of the actuation-redundant PKM is not so much superior to the non-redundant PKM. Moreover, in the middle segment of the trajectory, the condition numbers of the two machines are relatively large, which indicates that their performance will be all-low in this region.

Their tracking errors are shown in Figs. 31 and 32, respectively. It shows that because of the poor performance of matrix *R*, the position errors of the moving platform are not compensated well
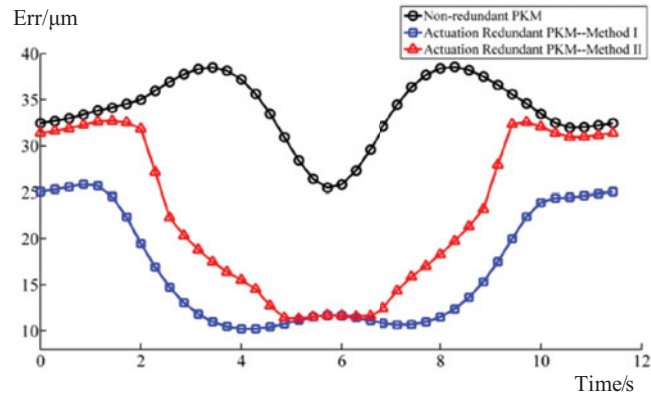
Fig. 28. Total position errors of the machines when running the new circular trajectory.
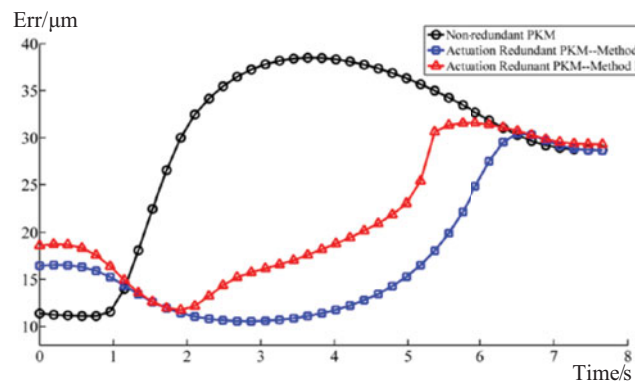
Fig. 29. Total position errors of the machines when running the line trajectory.
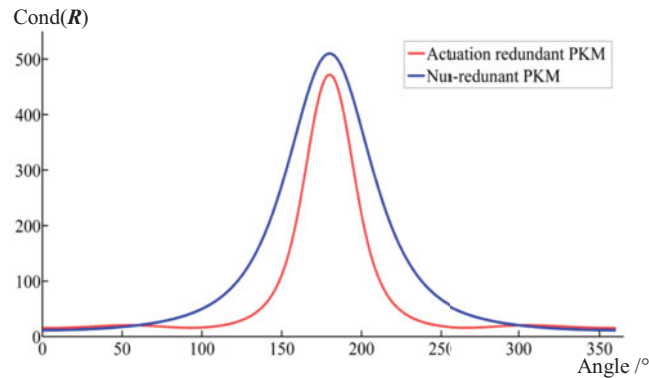
Fig. 30. Condition numbers of the position precision matrixes in expanded trajectory.

although the actuation redundancy is added. At this moment, it is necessary to optimize the structure and the running trajectory of the machine further.

6. Conclusion
This paper studies the dynamic modeling and proposes a novel method for redundant-force optimization of a planar 2-DOF PKM with actuation redundancy. This method is aiming at improving the position precision of the moving platform during operation, and solving the dynamic model constructed by the Newton–Euler method. Then the dynamic performance of this machine and its non-redundant counterpart is investigated by numerical examples. Their performance of the position precision matrixes, position and tracking errors, the driving parameters, and constraint forces are
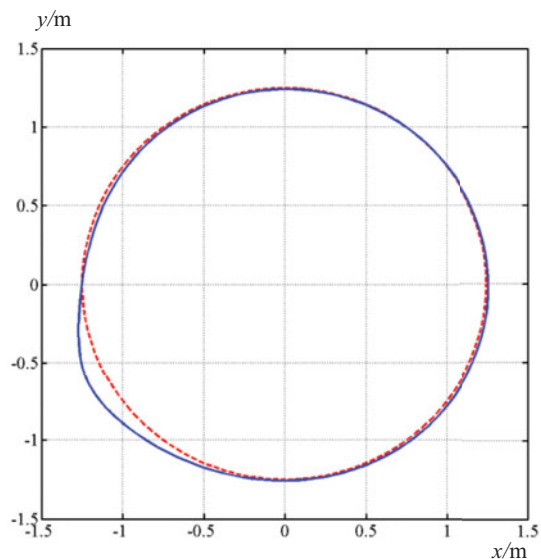
Fig. 31. Tracking error of the non-redundant PKM.
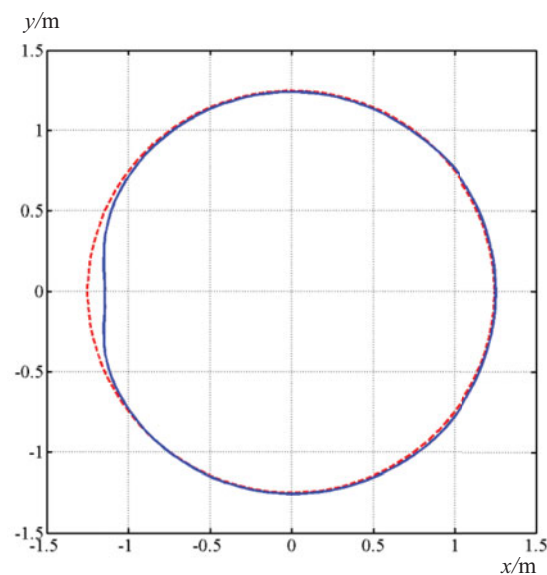
Fig. 32. Tracking error of the actuation-redundant PKM.

analyzed. Besides, another redundant-force optimization method for minimizing the constraint forces is also applied for comparison. Finally, insufficiently optimized redundant force in improving the position precision of the machine is provided, and further work on the optimization of the actuation-redundant PKM is proposed. The following conclusions can be drawn:

1. The optimization of the redundant force, which aims to minimize the position errors of the moving platform, can be used as a reasonable supplementary to solve the dynamic model.
2. The performance analysis of the position precision matrixes shows that the addition of the redundant kinematic chain is beneficial to the improvement of the machine's capability of resisting deformation in some cases.
3. The simulation analyses of the two machines when running the smaller circular trajectory show that the optimized redundant force can better compensate the position errors of the moving platform caused by the deformation of the links. The maximum position error is reduced from 32 μm to less than 12 μm.

4. The optimization method for minimizing the constraint forces contributes to reduce the constraint forces of joints compared with the novel method, while the position errors of the machine are always larger during operation, especially when the machine is suffering external load.

5. When the performance of the position precision matrix is poor, it will be difficult to compensate the position errors of the machine even though the actuation redundancy is applied. It is essential to optimize the structure and running trajectory of the machine further to improve its performance.

The analyses and comparison study have proved the effectiveness of the novel method in the dynamic model solving and the redundant-force optimization to improve the position precision of the actuation-redundant PKMs to a certain extent.

References
1. J. P. Merlet, *Parallel Robots*, 2nd ed. (Kluwer Academic Publishers, Dordrecht, 2005).
2. I. Ebrahimi, J. A. Carretero and R. Boudreau, "3-PRRR redundant planar parallel manipulator: Inverse displacement, workspace and singularity analyses," *Mech. Mach. Theory* **42**(8), 1007–1016 (2007).
3. Y. J. Zhao, F. Gao, W. M. Li and X. C. Zhao, "Development of a 6-DOF parallel seismic simulator with novel redundant actuation," *Mechatronics* **19**(3), 422–427 (2009).
4. Y. J. Zhao and F. Gao, Dynamic formulation and performance evaluation of the redundant parallel manipulator," *Robot. Comput.-Integr. Manuf.* **25**(4–5), 770–781 (2009).
5. J. Kim, F. C. Park, S. J. Ryu, "Design and analysis of a redundantly actuated parallel mechanism for rapid machining," *IEEE Trans. Robot. Autom.* **17**(4), 423–434 (2001).
6. A. Müller and T. Hufnagel "Model-based control of redundantly actuated parallel manipulators in redundant coordinates," *Robot. Auton. Syst.* **60**(4), 563–571 (2012).
7. H. Cheng, Y. K. Yiu and Z. X. Li "Dynamics and control of redundantly actuated parallel manipulators," *IEEE-ASME Trans. Mechatronics* **8**(4), 483–491 (2003).
8. Y. J. Zhao and F. Gao "Dynamic performance comparison of the 8PSS redundant parallel manipulator and its non-redundant counterpart-the 6PSS parallel manipulator," *Mech. Mach. Theory* **44** (5), 991–1008 (2009).
9. S. B. Nokleby, R. Fisher, R. P. Podhorodeski and F. Firmani, "Force capabilities of redundantly actuated parallel manipulators," *Mech. Mach. Theory* **40**(5), 578–599 (2005).
10. A. Zibil, F. Firmani, S. B. Nokleby, R. P. Podhorodeski, "An explicit method for determining the force-moment capabilities of redundantly actuated planar parallel manipulators," *J. Mech. Des.* **129**(10), 1046–1055 (2007).
11. A. Müller, "Internal preload control of redundantly actuated parallel manipulators—It's application to backlash avoiding control," *IEEE Trans. Robot.* **21**(4), 668–677 (2005).
12. A. Fattah and G. Kasaei "Kinematics and dynamics of a parallel manipulator with a new architecture," *Robotica* **18**, 535–543 (2000).
13. B. Dasgupta and P. Choudhury "A general strategy based on the Newton–Euler approach for the dynamic formation of parallel manipulators," *Mech. Mach. Theory* **34**(6), 801–824 (1999).
14. J. Carvalho and M. Ceccarelli, "A closed-form formulation for the inverse dynamics of a Cassino parallel manipulator," *Multibody Syst. Dyn.* **5**(2), 185–210 (2001).
15. W. Khalil and S. Guegan, "Inverse and direct dynamic modeling of Gough-Stewart robots," *IEEE Trans. Robot. Autom.* **20**(4), 754–762 (2004).
16. H. Abdellatif and B. Heimann, "Computational efficient inverse dynamic of 6-DOF fully parallel manipulators by using the Lagrangian formalism," *Mech. Mach. Theory* **44**(1), 192–207 (2009).
17. R. Di Gregorio and V. Parenti-Castelli, "Dynamics of a class of parallel wrists," *J. Mech. Des*. **126**(3), 436–441 (2004).
18. M. Callegari, M. C. Palpacelli and M. Principi, "Dynamics modelling and control of the 3-RCC translational platform," *Mechatronics* **16**(10), 589–605 (2006).
19. L. W. Tsai, "Solving the inverse dynamics of a Stewart–Gough manipulator by the principle of virtual work," *J. Mech. Des.* **122**(1), 3–9 (2000).
20. M. J. Liu, C. X. Li and C. N. Li, "Dynamics analysis of the Gough-Stewart platform manipulator," *IEEE Trans. Robot. Autom.* **16**(1), 94–98 (2000).
21. G. Cheng and X. L. Shan, "Dynamic analysis of a parallel hip joint simulator with four degree of freedoms (3R1T)," *Nonlinear Dyn.* **70**(4), 2475–2486 (2012).
22. J. Gallardo, J. M. Rico, A. Frisoli, D. Checcacci and M. Bergamasco, "Dynamics of parallel manipulators by means of screw theory," *Mech. Mach. Theory* **38**(11), 1113–1131 (2003).

23. Y. F. Zheng and J. Y. S. Luh, "Optimal load distribution for two industrial robots handling a single object," *Trans. ASME, J. Dyn. Syst. Meas. Control* **111**(2), 232–237 (1989).
24. J. M. Tao, J. Y. S. Luh, "Coordination of Two Redundant Manipulators," *Proceedings of the 1989 IEEE International Conference on Robotics and Automation*, Scottsdale, USA (May 14–19, 1989) pp. 425–430.
25. M. Nahon and J. Angeles, "Optimization of dynamic forces in mechanical hands," *J. Mech. Des.* **113**(2), 167–173 (1991).
26. J. P. Merlet, "Redundant parallel manipulators," *Lab. Robot. Autom.* **8**(1), 17–24 (1996).
27. V. Garg, S. B. Nokleby and J. A. Carretero, "Wrench capability analysis of redundantly actuated spatial parallel manipulators," *Mech. Mach. Theory* **44**(5), 1070–1081 (2009).
28. S. H. Lee, J. H. Lee, B. J. Yi, S. H. Kim and Y. K. Kwak, "Optimization and experimental verification for the antagonistic stiffness in redundantly actuated mechanisms: a five-bar example," *Mechatronics* **15**(2), 213–238 (2005).
29. X. Y. Wang and J. K. Mills, "Dynamic modeling of a flexible-link planar parallel platform using a substructuring approach," *Mech. Mach. Theory* **41**(6), 671–687 (2006).
30. S. Tzafestas, M. Kotsis and T. Pimenides, "Observer-based optimal control of flexible Stewart parallel robots," *J. Intell. Robot. Syst.* **34**(4), 489–503 (2001).
31. H. D. Taghirad and M. A. Nahon, "Dynamic analysis of a macro-micro redundantly actuated parallel manipulator," *Adv. Robot.* **22**(9), 949–981 (2008).
32. J. Wu, J. S. Wang, T. M. Li and L. P. Wang, "Dynamic analysis of the 2-DOF planar parallel manipulator of a heavy duty hybrid machine tool," *Int. J. Adv. Manuf. Technol.* **34**(3–4), 413–420 (2007).